The Chaotic Response of a Fluttering Panel: The Influence of Maneuvering

SLOBODAN R. SIPCIC

Department of Aerospace and Mechanical Engineering, Boston University, Boston MA 02215, U.S.A.

Abstract. The influence of maneuvering on the chaotic response of a fluttering buckled plate on an aircraft has been studied. The governing equations, derived using Lagrangian mechanics, include geometric non-linearities associated with the occurrence of tensile stresses, as well as coupling between the angular velocity of the maneuver and the elastic degrees of freedom. Numerical simulation for periodic and chaotic responses are conducted in order to analyze the influence of the pull-up maneuver on the dynamic behavior of the panel. Long-time histories, phase-plane plots, and power spectra of the responses are presented. As the maneuver (load factor) increases, the system exhibits complicated dynamic behavior including a direct and inverse cascade of subharmonic bifurcations, intermittency, and chaos. Beside these classical routes of transition from a periodic state to chaos, our calculations suggest amplitude modulation as a possible new mode of transition to chaos. Consequently this research contributes to the understanding of the mechanisms through which the transition between periodic and strange attractors occurs in dissipative mechanical systems. In the case of a prescribed time dependent maneuver, a remarkable transition between the different types of limit cycles is presented.

Key words: Aeroelastic flutter, influence of maneuvering, chaotic vibrations, routes to chaos, dissipative dynamical systems, computational methods.

Nomenclature

a	= plate length
a_r	= u_r/h
D	= plate bending stiffness
E	= modulus of elasticity
g	= acceleration due to gravity
h	= plate thickness
$\mathbf{j}_1, \mathbf{j}_2, \mathbf{j}_3$	= base vectors of the body frame of reference
K	= spring constant
M	= Mach number
n	= $1 + \omega v_0/g$
N_x	= applied in-plane force
$p - p_\infty$	= aerodynamic pressure
P	= $\Delta p a^4/Dh$
q	= $\rho v_0^2/2$
Q_r	= generalized Lagrangian forces
$\mathbf{R}$	= rotation matrix
R_x	= $N_x a^2/D$
t	= time
$\mathcal{T}$	= kinetic energy
u	= plate deflection
$\mathbf{u}$	= displacement of the structure
u_r	= modal amplitude
$\mathbf{v}_0$	= velocity
$\mathbf{x}$	= coordinates in the inertial frame of reference
$\mathbf{z}$	= coordinates in the body frame of reference
α	= $Ka/(Ka + Eh)$
β	= $\sqrt{M^2 - 1}$
ε	= elastic energy
λ	= $2qa^3/\beta D$

Nonlinear Dynamics **1**: 243–264, 1990

μ = $\rho a/\rho_m h$
ν = Poisson's ratio
ξ^α = material coordinates
ρ = air density
ρ_m = plate density
τ = $t\sqrt{D/\rho_m h a^4}$
$\boldsymbol{\phi}_r$ = prescribed functions
ϕ_r = $\sin(r\pi z/a)$
ω = angular velocity
Ω = $\omega a/v_0$
$\mathbf{\Omega}$ = skew-symmetric matrix form of the angular velocity

1. Introduction

This paper deals with the chaotic behavior of a fluttering panel on a maneuvering airplane. Such a system is interesting from the dynamic point of view because it combines a maneuver (which manifests itself as forced excitations, as well as more complicated coupling, including parametric excitation), and flow-induced oscillations on a system with two fixed points (buckled plate). As a result of combining the force-induced and flow-induced oscillations, this system is a rich source of static and dynamic instabilities and of associated limit-cycle motions. In the past, several approaches have been used for the separate treatment of these problems. Very simple models have been used for the simple problem of the forced vibration of a buckled plate (essential to the understanding of the more complicated system under consideration, Dowell and Ilgamov, [4]). For example, in Dowell and Pezeshki [5], and Pezeshki and Dowell [8], and [9], Duffing's equation has been used as a model for the sinusoidally excited buckled plate. Yano [14], and [15] investigated different cases of a van der Pol–Mathieu type equation used to model a beam subjected to a periodic axial force and simultaneously to a flow-induced vibration. He included quadratic and cubic non-linearities in the parametric term and only cubic non-linearities in the restoring force. Zavodney and Nayfeh [10], and Zavodney *et al.* [11], analyzed the response of a one degree of freedom system with quadratic and cubic non-linearities to a fundamental harmonic parametric excitation. They found solutions characterized by period multiplying bifurcations and chaos. For the problem under consideration, the non-linear partial differential equation is approximated, by Galerkin or Rayleigh–Ritz methods, as a set of ordinary differential equations which are then solved for specific initial conditions by numerical integration techniques. An excellent review of the work using this approach is given in Dowell and Ilgamov [4]. A dissipative partial differential equation modeling a buckled beam was considered by Holmes and Marsden [6]. They presented one of the very few analytical results available on chaos in a continuous system.

We are interested here in highly maneuverable aircraft. One feature of these aircraft is that the angular velocity can be much higher than in more conventional aircraft. As a consequence, a body frame of reference connected with the aircraft cannot be assumed to be in pure translation, and the governing equations should be written in a rotating frame of reference. This implies that there is a coupling between the rigid-body and the flexible-body motion. Note that the effect of maneuvering on the dynamic response of a fluttering panel is not discussed by Dowell and Ilgamov [4]. The influence of maneuvering on a periodic response of a fluttering buckled plate was analyzed by Sipcic and Morino [12], and [13]. The current paper deals with the chaotic behavior of a fluttering panel on a maneuvering plane.

The study has been divided into two main areas, theoretical and numerical. In Section 2 the governing equations are derived in the 'body' frame of reference following the procedure of Lagrangian mechanics. Numerical results are presented in Section 3. The governing equations are integrated numerically, using a fourth-order Runge–Kutta algorithm. In order to understand the dynamics, the character of the solution has been examined, in physical terms, in Subsection 3.1. The effect of varying the load factor was studied in great detail, only representative results are presented in Subsection 3.2. In examining and discussing the results, attention is drawn to the routes to chaos. Long time histories, phase-plane plots, and power spectra of the responses were the dynamics tools used to study the system considered here. Finally, a prescribed time dependent maneuver is considered in Subsection 3.3.

2. The Equation of Motion

Consider a thin plate having length a, thickness h, and undergoing cylindrical bending in response to one sided airflow, see Figure 1. As mentioned before the plate motion is expressed in terms of the rigid-body translation and rotation of the body reference frame, and a deformation. Indicating the coordinates in the inertial frame with $\mathbf{x}$, the coordinates of the origin P_0 of the body frame with $\mathbf{x}_0$, the body-axis coordinates of a point P in the body frame at time $t = 0$ (reference condition) with $\mathbf{z}$, and the body-axis components of the displacement of the structure with respect to a reference condition with $\mathbf{u}$, we have

$$\mathbf{x}(\xi^\alpha, t) = \mathbf{x}_0(t) + \mathbf{R}(t)[\mathbf{z}(\xi^\alpha) + \mathbf{u}(\xi^\alpha, t)]\,, \tag{1}$$

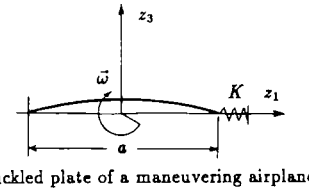

Buckled plate of a maneuvering airplane

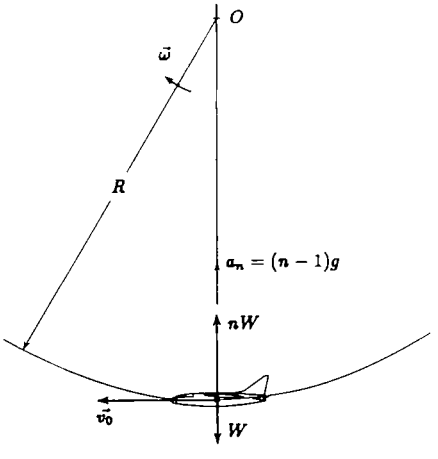

Fig. 1. Airplane in a pull-up.

where ξ^α is a system of material coordinates (i.e., a system of coordinates, in general curvilinear, that is convected with the material point). Typically, these coincide numerically with the components z_i of $\mathbf{z}$. Note that the matrix $\mathbf{R}$ represents a rigid-body rotation. Next let us assume that a deformation is given as a linear combination of prescribed functions, $\boldsymbol{\phi}_r$, with unknown coefficients, i.e.,

$$\mathbf{u}(\xi^\alpha, t) = \sum_r u_r(t)\boldsymbol{\phi}_r(\xi^\alpha) . \tag{2}$$

In the rest of this section the equations of motion for the elastic degree of freedom, u_r, are obtained by the use of Lagrange's equations in the form

$$\frac{\mathrm{d}}{\mathrm{d}t}\frac{\partial \mathcal{T}}{\partial \dot{u}_r} - \frac{\partial \mathcal{T}}{\partial u_r} + \frac{\partial \varepsilon}{\partial u_r} = Q_r , \tag{3}$$

where $\mathcal{T}$ is the kinetic energy, ε is the elastic energy, and Q_r are the generalized Lagrangian forces.

2.1. *Kinetic Energy*

The kinetic energy is given by

$$\mathcal{T} = \frac{1}{2}\iiint_V \rho \|\mathbf{v}\|^2 \,\mathrm{d}V . \tag{4}$$

The velocity $\boldsymbol{v}$ of a point ξ^α may be obtained from Equation 1, as

$$\boldsymbol{v}(\xi^\alpha, t) = \frac{\partial \mathbf{x}}{\partial t}\bigg|_{\xi^\alpha} = \dot{\mathbf{x}}_0(t) + \mathbf{R}(t)\{\boldsymbol{\Omega}(t)[\mathbf{z}(\xi^\alpha) + \mathbf{u}(\xi^\alpha, t)] + \dot{\mathbf{u}}(\xi^\alpha, t)\} , \tag{5}$$

where $\boldsymbol{\Omega}$ is the skew-symmetric matrix form of the angular velocity, and $\dot{\mathbf{x}}_0(t)$ is the velocity $\mathbf{v}_0$ of the origin P_0 coordinatized in the inertial frame of reference. In what follows the constant velocity pull-up maneuver will be assumed. If the base vectors of the body frame of reference are $\mathbf{j}_1, \mathbf{j}_2, \mathbf{j}_3$, see Figure 1, then $\mathbf{v}_0 = -v_0\mathbf{j}_1$, and the angular velocity $\boldsymbol{\omega} = -\omega\mathbf{j}_2$. Furthermore, the prescribed functions $\boldsymbol{\phi}_r$ are all in the direction $\mathbf{j}_3$. Making use of these assumptions and substituting (2) and (5) into (4) it is found that

$$\mathcal{T} = \frac{1}{2}mv_0^2 + \frac{1}{2}\omega^2\sum_{r,s} m_{rs}u_r u_s - v_0\omega\sum_r s_r u_r + \frac{1}{2}\omega^2 J_0 + \frac{1}{2}\sum_{r,s} m_{rs}\dot{u}_r\dot{u}_s + \omega\sum_r b_r\dot{u}_r , \tag{6}$$

where,

$$m = \iiint_V \rho \,\mathrm{d}V \qquad m_{rs} = \iiint_V \rho\phi_r\phi_s \,\mathrm{d}V \qquad b_r = \iiint_V \rho z\phi_r \,\mathrm{d}V$$

$$s_r = \iiint_V \rho\phi_r \,\mathrm{d}V \qquad J_0 = \iiint_V \rho z^2 \,\mathrm{d}V . \tag{7}$$

Substituting (6) into (3) the equations of motion become

$$s_r\omega v_0 + b_r\dot{\omega} + \sum_s m_{rs}\ddot{u}_s - \sum_s \omega^2 m_{rs}u_s + \frac{\partial \varepsilon}{\partial u_r} = Q_r . \tag{8}$$

2.2. Elastic Energy

Consider once more a thin two-dimensional, simply supported plate having length a and thickness h and undergoing cylindrical bending in response to one sided airflow, see Figure 1. In such a case the axial extension, v, can be written to first order approximation as

$$v(z) = -\frac{1}{2}\int_0^z \left(\frac{\partial u}{\partial z}\right)^2 \mathrm{d}z \,. \tag{9}$$

Thus the elastic energy is

$$\varepsilon = \frac{D}{2}\int_0^a \left(\frac{\partial^2 u}{\partial z^2}\right)^2 \mathrm{d}z + \frac{\alpha Eh}{2a}\left[\frac{1}{2}\int_0^a \left(\frac{\partial u}{\partial z}\right)^2 \mathrm{d}z\right]^2, \tag{10}$$

where D is a plate bending stiffness, α is a support factor which accounts for the effective stiffness of the supporting structure defined by

$$\alpha = \frac{Ka}{Ka + Eh} \tag{11}$$

and K is a spring constant per unit spanwise length of panel. Substituting (2) into the elastic energy, Equation 10, and differentiating with respect to u_r one obtains

$$\frac{\partial \varepsilon}{\partial u_r} = D\sum_s e_{rs}u_s + \frac{\alpha Eh}{2a}\sum_{s,m,l} k_{rsml}u_s u_m u_l \,, \tag{12}$$

where

$$k_{rsml} = \int_0^a \phi_s'\phi_m' \,\mathrm{d}z \int_0^a \phi_l'\phi_r' \,\mathrm{d}z \qquad e_{rs} = \int_0^a \phi_s''\phi_r'' \,\mathrm{d}z \,. \tag{13}$$

2.3. Generalized Lagrangian Forces

Assume that the plate is exposed to an in-plane tensile load, N_x, to a static pressure difference across the plate, ΔP, and that the exciting dynamic pressure difference is given by quasi-steady aerodynamic theory, i.e. (see Bisplinghoff and Ashley [1]),

$$p - p_\infty = \frac{2q}{\beta}\left[\frac{\partial u}{\partial z} + \frac{M^2 - 2}{M^2 - 1}\frac{1}{v_0}\frac{\partial u}{\partial t}\right], \tag{14}$$

where $q = \rho v_0^2/2$ is the dynamic pressure, M is the Mach number, and $\beta = \sqrt{M^2 - 1}$. Following the conventional procedure of Lagrangian mechanics, i.e., calculating the virtual work performed by the external forces as they act through the virtual displacement caused by the variation in the generalized coordinate u_r, the expression for the generalized force Q_r is

$$Q_r = -N_x\sum_s n_{rs}u_s + \Delta P p_r - \frac{2q}{\beta}\sum_s (u_s p_{rs} + \dot{u}_s \hat{p}_{rs}) \,, \tag{15}$$

where

$$n_{rs} = \int_0^a \phi_r' \phi_s' \, dz \qquad p_r = \int_0^a \phi_r \, dz \qquad p_{rs} = \int_0^a \phi_r \phi_s' \, dz \qquad \hat{p}_{rs} = \frac{\beta^2 - 1}{\beta^2 v_0} \int_0^a \phi_r \phi_s \, dz \,. \tag{16}$$

Substituting (12) and (15) into the equations of motion (8), one obtains

$$s_r \omega v_0 + b_r \dot{\omega} + \sum_s m_{rs} \ddot{u}_s - \sum_s \omega^2 m_{rs} u_s + D \sum_s e_{rs} u_s + \frac{\alpha E h}{2a} \sum_{s,m,l} k_{rsml} u_s u_m u_l + N_x \sum_s n_{rs} u_s$$
$$+ \frac{2q}{\beta} \sum_s (u_s p_{rs} + \dot{u}_s \hat{p}_{rs}) = \Delta P p_r \,. \tag{17}$$

2.4. Dimensionless Equations

In order to recast Equation 17 in a dimensionless form, we introduce the following dimensionless parameters and coordinates:

$$a_r = \frac{u_r}{h} \qquad \tau = t\left(\frac{D}{\rho_m h a^4}\right)^{1/2} \qquad \Omega = \frac{\omega a}{v_0} \qquad \lambda = \frac{2qa^3}{\beta D} \qquad R_x = \frac{N_x a^2}{D} \qquad P = \frac{\Delta P a^4}{Dh}$$
$$\mu = \frac{\rho a}{\rho_m h} \,. \tag{18}$$

Furthermore, since the plate is simply supported, we will allow the prescribed functions to be

$$\phi_r = \sin(r\pi z/a) \,. \tag{19}$$

Substituting Equation 19 into (7), (13), and (16), and thence into (17), the equation of motion in dimensionless matrix form reads

$$\ddot{\mathbf{a}} + \delta \dot{\mathbf{a}} + \mathbf{G}\mathbf{a} + \mathbf{f}(\mathbf{a}) + \gamma \Omega^2 \mathbf{a} = \mathbf{p} + \dot{\Omega}\mathbf{d} + \Omega \mathbf{v} \,, \tag{20}$$

where $\mathbf{a} = \{a_r\}$, $\boldsymbol{G} = [g_{rs}]$, $\mathbf{d} = \{d_r\}$, $\mathbf{v} = \{v_r\}$, $\mathbf{p} = \{p_r\}$, $\mathbf{f} = \{f_r\}$, and

$$g_{rs} = 2\lambda \frac{rs}{r^2 - s^2}[1 - (-1)^{r+s}] + [(r\pi)^2 R_x + (r\pi)^4]\delta_{rs} \qquad \delta = \frac{\beta^2 - 1}{\beta^2}\left(\frac{\lambda\mu}{M}\right)^{1/2}$$
$$d_r = -2\frac{(-1)^r}{\pi r}\left(\frac{\beta\lambda}{\mu}\right)^{1/2}\frac{a}{h}$$
$$v_r = -2\frac{\beta\lambda}{\mu}\frac{a}{h}\frac{[1-(-1)^r]}{\pi r} \qquad p_r = 2P\frac{[1-(-1)^r]}{\pi r} \qquad \gamma = -\frac{\beta\lambda}{\mu}$$
$$f_r = 3r^2\pi^4\alpha(1-\nu^2)a_r \sum_s s^2 a_s^2 \,, \tag{21}$$

with $s, r = 1, \ldots, N$. Equations 20 are a set of ordinary, nonlinear differential equations in time. The cubic non-linearities are of geometric origin and are associated with the occurrence of tensile stresses in the middle surface. The coupling between the rigid-body rotation of the frame of reference and the elastic degrees of freedom is represented by the fifth term. This set of equations have been solved by a direct numerical integration. Note that by assuming $\Omega = 0$, Equations 20 properly reduce to the classical panel flutter equations (see e.g., Bolotin [2], or Dowell [3]).

3. Numerical Experimentation

In this research numerical simulations are conducted in order to analyze the chaotic behavior of a fluttering panel on a maneuvering airplane. Equations 20 are simulated on the digital computer using a fourth order Runge–Kutta algorithm. For the sake of clarity, the factor Ω is expressed in terms of the load factor $n = 1 + \omega v_0/g$, as $\Omega = (n-1)ag/v_0^2$. The load factor for aeronautical applications is in the range 1 to 6. For all of the results reported here, $\mu/M = 0.023$, $\alpha = 1$, $\nu = 0.3$, $h/a = 0.008$, $M = 1.3$, $ag/v_0^2 = 1.45 \times 10^{-5}$, and the plate response is calculated at $z/a = 0.75$. In order to eliminate the influence of the initial conditions from the maneuvering, the same initial conditions are prescribed for all cases by setting, $\dot{a}_1 = 1.0$ (corresponding to a positive velocity of the first degree of freedom). Previous calculations of Paolozzi, Peroni, and Sipcic [7] have shown that at least six degrees of freedom (i.e., number of modes) has to be used in order to properly capture the dynamic behavior of the system. This is why the computations presented here are performed using six degrees of freedom.

3.1. Character of the Solution in the Presence of a Maneuver

For the sake of clarity, before addressing the general results, the key types of responses are introduced from a physical point of view. The buckled plate is a part of the maneuvering airplane (see Figure 1). Depending on the value of the load factor and other parameters, one or two stable fixed points may be obtained in the phase plane $(u, \dot{u})$. The first fixed point corresponds to the undeformed position, the other two to the up buckled or down buckled plate position. The stable plate motion, generally speaking, consists of vibration around up buckled, down buckled position, and 'snapping through' motion.

Figure 2 shows selected phase-plane plots of the panel responses in the non-maneuvering case. When the buckled plate is excited by the one sided airflow, one finds one global limit cycle orbit around both buckled fixed points, and three more complicated periodic limit cycles, see Dowell [4], or Paolozzi, Peroni, and Sipcic [7]. In the first case of simple harmonic response the plate is 'snapping through' around both buckled positions. More complicated periodic response are combination of the plate vibration around up buckled, or down buckled position, and 'snapping through' motion.

Influence of the maneuver on the periodic plate response has been studied by Sipcic and Morino [12], and [13]. In order to perform the maneuver an airplane has to be exposed to normal force, i.e., another parameter of interest is the uniform static pressure differential across the plate. In the absence of a maneuver, the plate would deform to some static equilibrium position under the pressure differential. While maneuvering, the inertial forces due to the maneuver decrease the deformation of the plate due to the static pressure differential. For sufficiently large flow velocity, this equilibrium position becomes unstable. The plate then begins to oscillate about the unstable equilibrium position, eventually reaching a new stable dynamic equilibrium shape (a limit cycle). A variety of limit cycles may be found as shown in Sipcic and Morino [12], [13]. A particularly important finding is that in the range $\lambda = 353$ to 361 the occurrence of a maneuver can change the character of the panel response from a fixed point in the non-maneuvering case ($n = 1$), to a limit cycle in the maneuvering case ($n = 2$), (see Figure 3). The maneuver can also suppress the periodic character of the motion, transforming the response into a fixed point, and all motion ceases. Finally, there is also the possibility of a chaotic response, but these will be discussed in what follows.

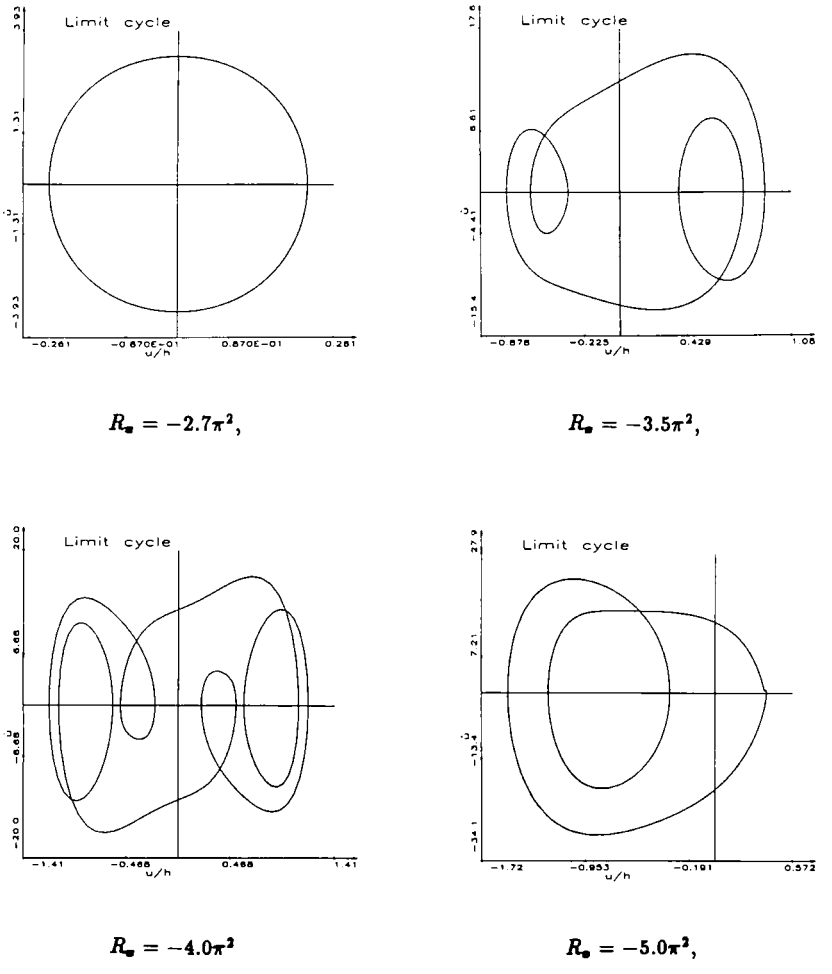

$R_x = -2.7\pi^2$, $R_x = -3.5\pi^2$,

$R_x = -4.0\pi^2$ $R_x = -5.0\pi^2$,

Fig. 2. Representative phase plane orbits for $\lambda = 150$, $n = 1.00$, and different values of in-plane loads.

3.2. *Routes to Chaos*

In the following we will discuss how maneuvering transforms the response from the steady state regime to the chaotic regime. The emphasis will be on the understanding of the mechanisms through which a chaotic regime establishes. We have chosen the system parameters such that there are two equilibrium positions for the non-maneuvering case. For this base case of $\lambda = 150$, and $R_x = -3.5\pi^2$, the load factor was varied from the non-maneuvering response to a value for which the inertial forces due to maneuvering suppress the plate motion, transforming the response into a fixed point. Figures 4(a) to 4(t) (discussed in details in the following subsections) shows the phase portraits of distinct attractors together with the power spectrum plots discovered during numerical experimentation. Time traces of selected responses are shown in Figure 5.

3.2.1. *Intermittency and Transient Chaos*

We begin with the non-maneuvering ($n = 1$) response shown in Figures 4(a) and 5(a). The motion has a nonchaotic character with three closed orbits in evidence. For the maneuvering case up to

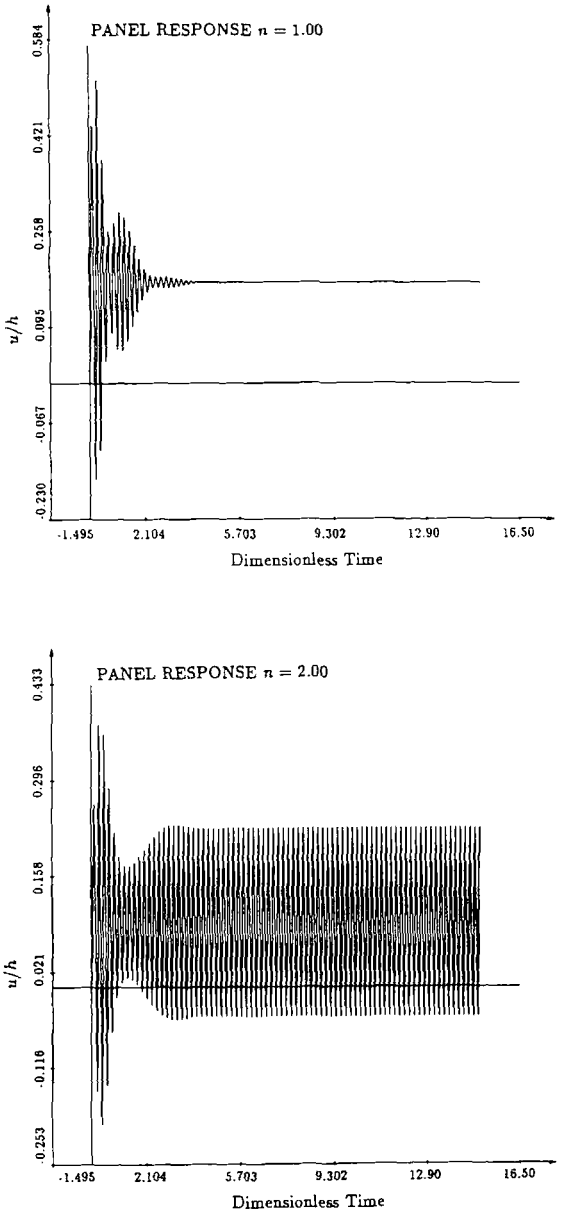

Fig. 3. Panel response for $\lambda = 355$, and $R_i = 0.0$, and $P = 60.0$.

$n = 1.66$, we see what appears to be a chaotic response. The power spectrum shows large fundamental frequency components accompanied by less broad band noise than that for the true chaotic response, see Figures 4(b) and 4(c). Furthermore, the time traces show the periodic motion with a short bursts of chaotic transient, see Figure 5(c). All this suggests that this is a region of transient chaos. At the value of the load factor $n = 1.67$, a new stable attractor appears (see Figure 4(d)), where the inertial forces due to maneuvering have suppressed one of the three orbits that appears for the non-maneuvering case. This trajectory experiences a cascade of

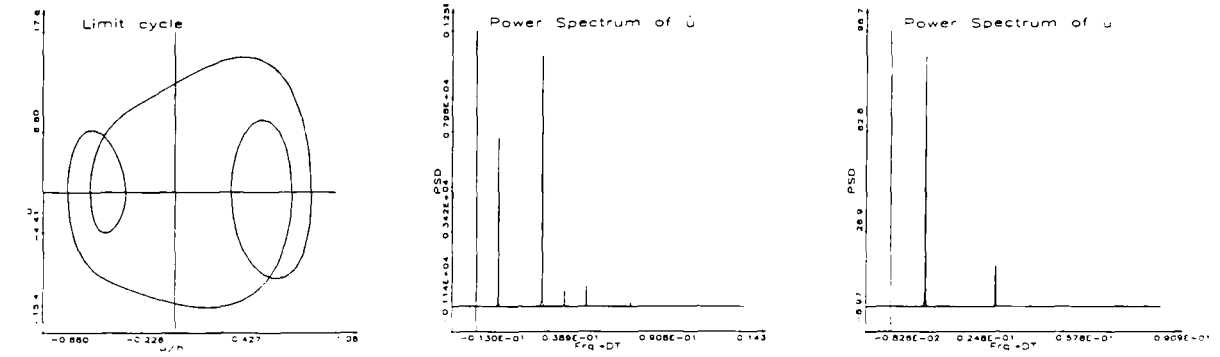

(a) Load factor $n = 1.00$

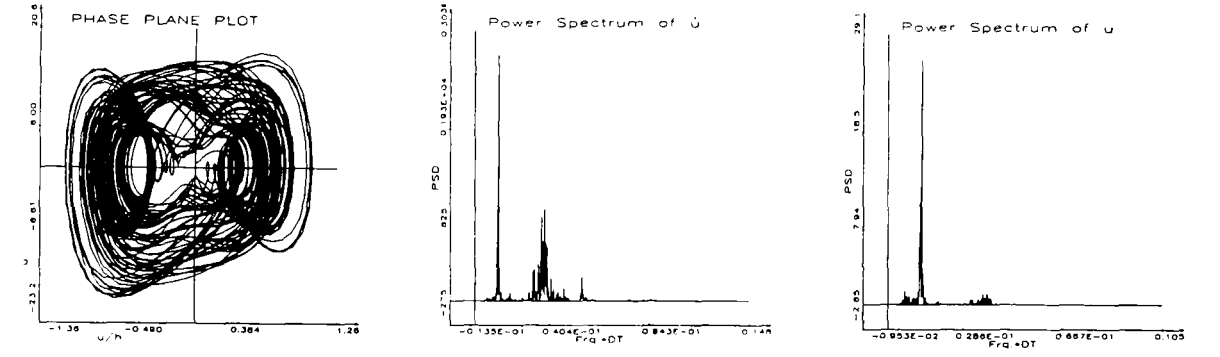

(b) Load factor $n = 1.28$

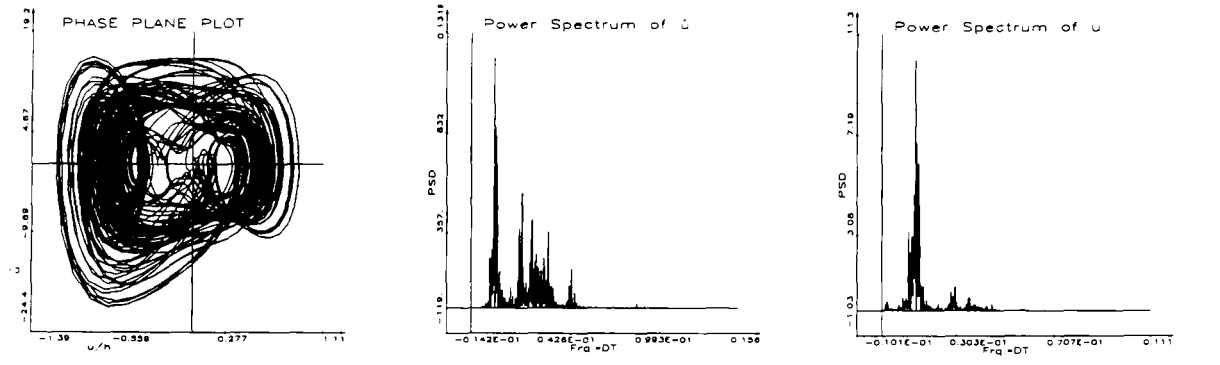

(c) Load factor $n = 1.66$

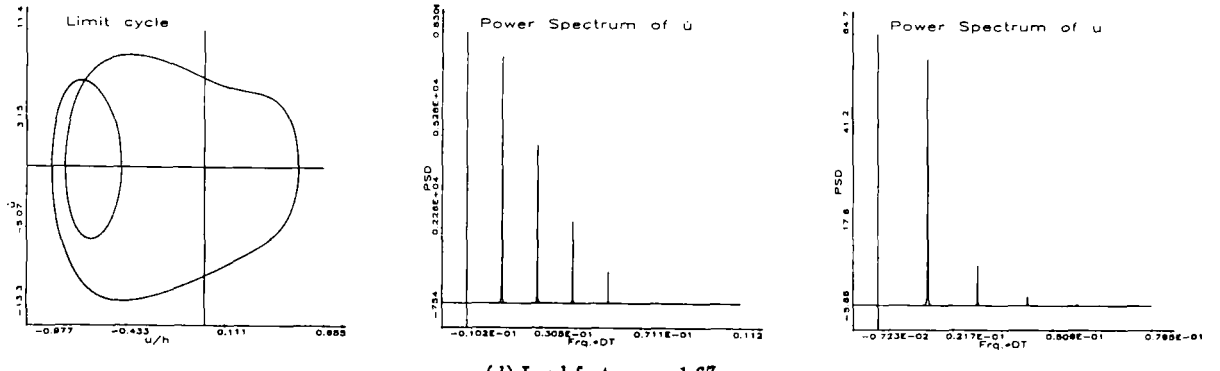

(d) Load factor $n = 1.67$

Fig. 4. Phase-plane portraits and the accompanying frequency spectra of the system response. The maneuver varies from $n = 1.00$, to $n = 3.00$.

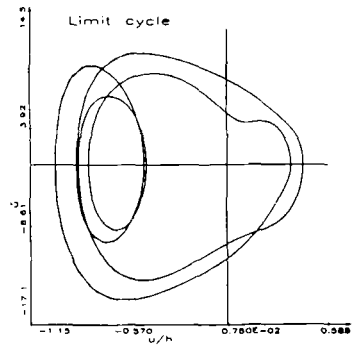

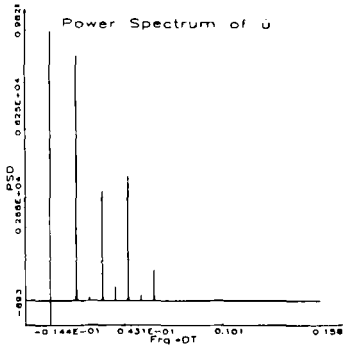

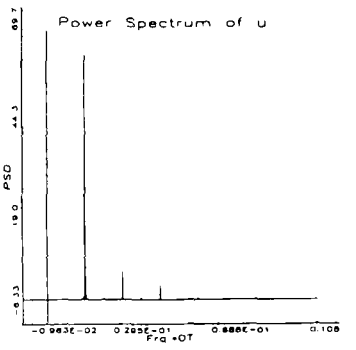

(e) Load factor $n = 1.83$

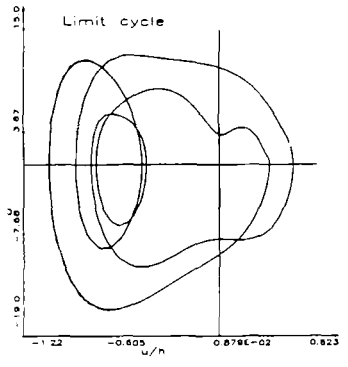

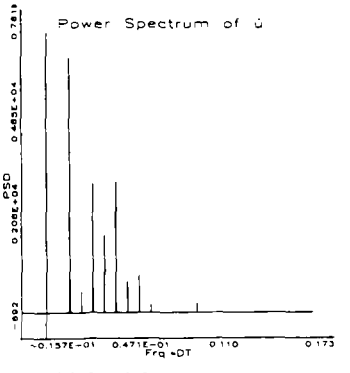

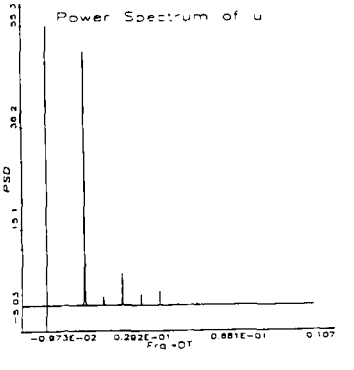

(f) Load factor $n = 1.90$

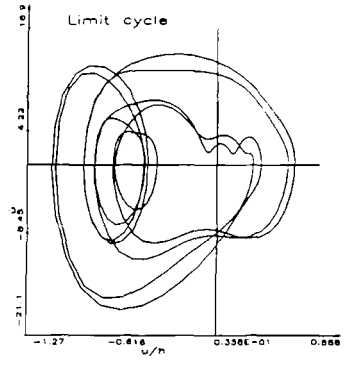

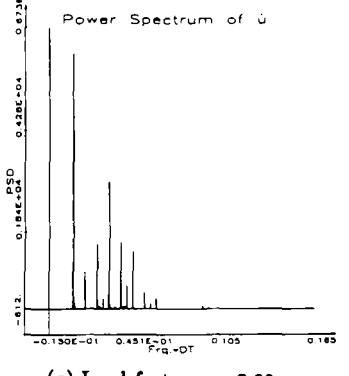

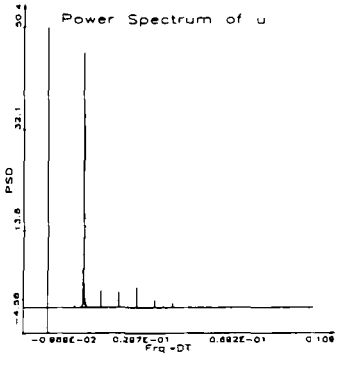

(g) Load factor $n = 2.00$

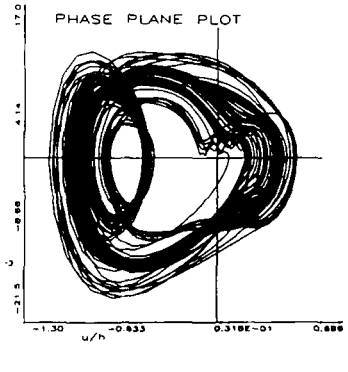

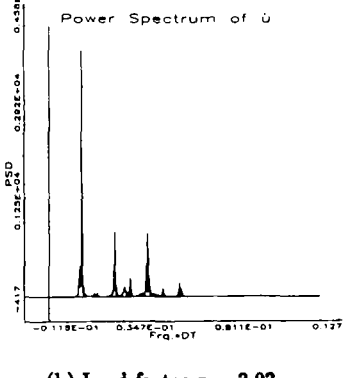

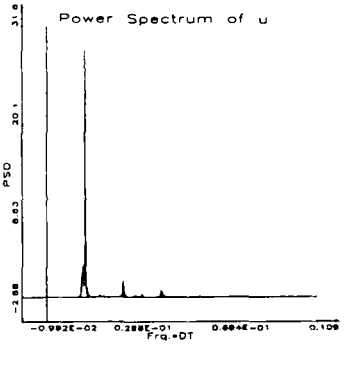

(h) Load factor $n = 2.02$

Figure 4. (continued).

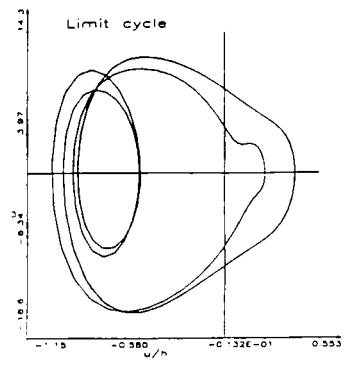

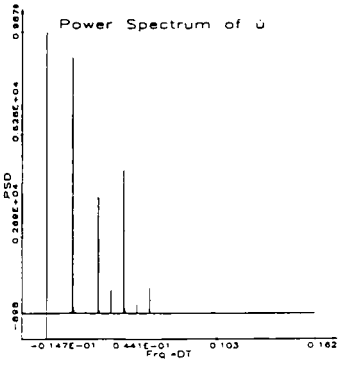

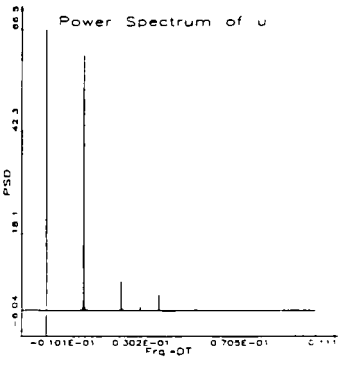

(i) Load factor $n = 2.03$

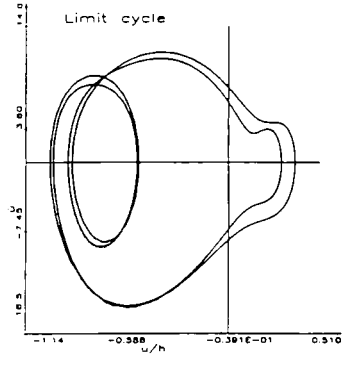

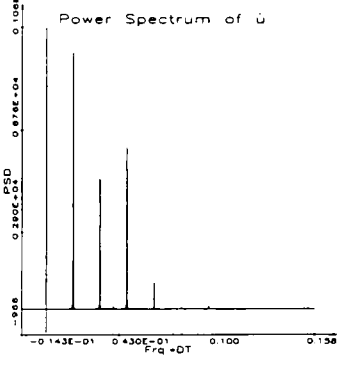

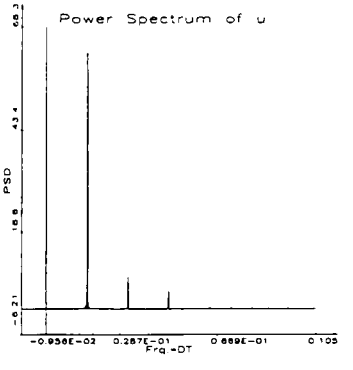

(j) Load factor $n = 2.18$

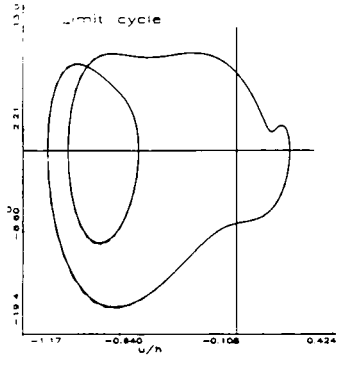

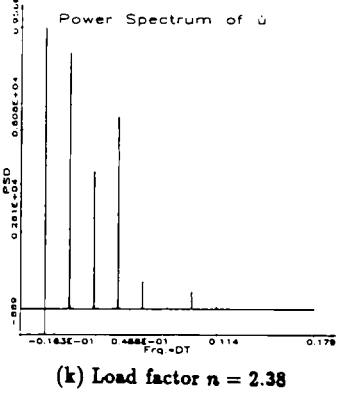

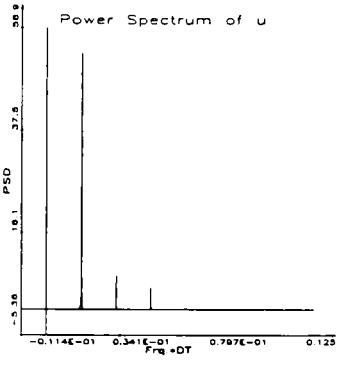

(k) Load factor $n = 2.38$

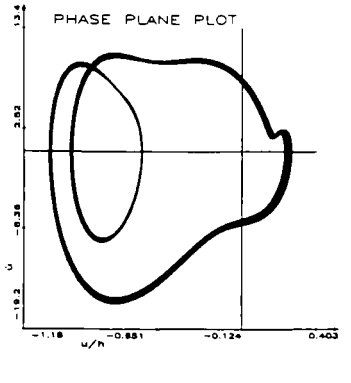

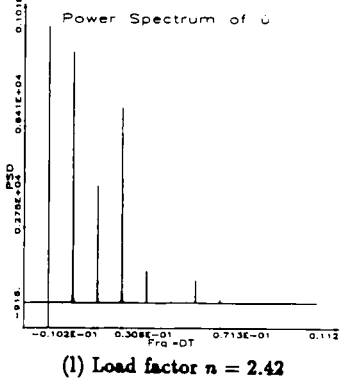

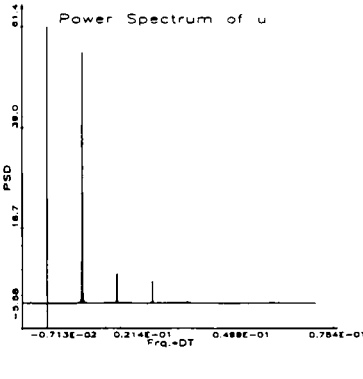

(l) Load factor $n = 2.42$

Figure 4. (continued).

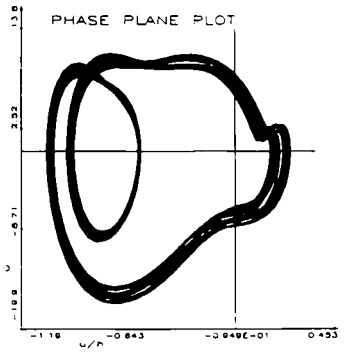

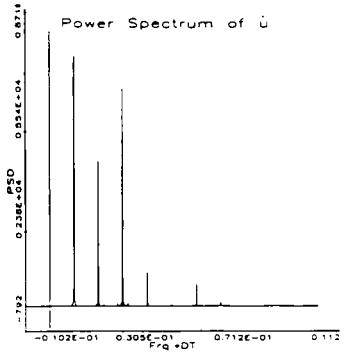

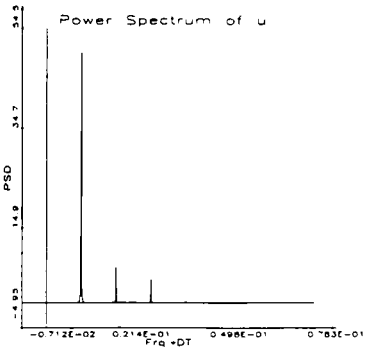

(m) Load factor $n = 2.44$

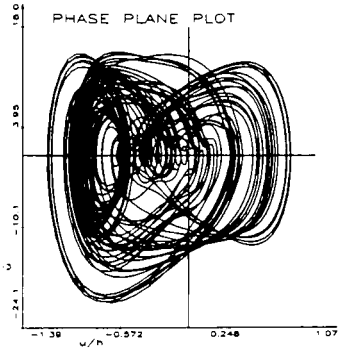

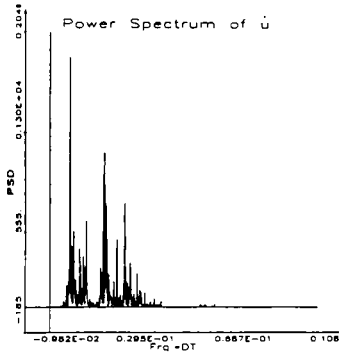

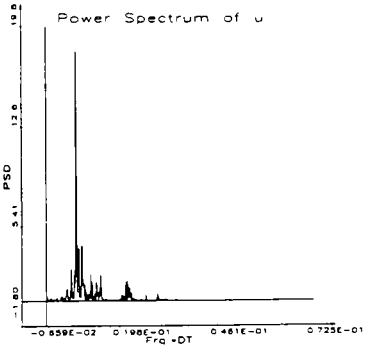

(n) Load factor $n = 2.48$

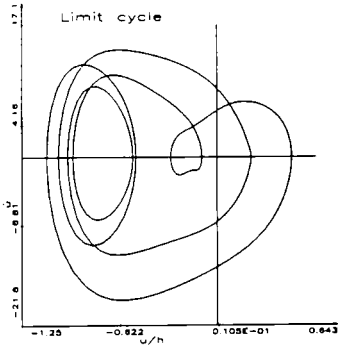

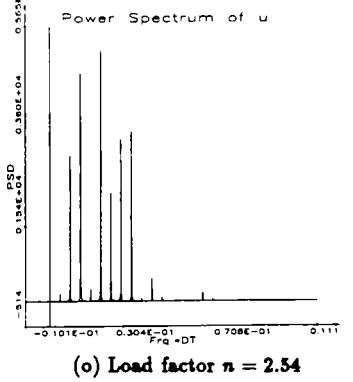

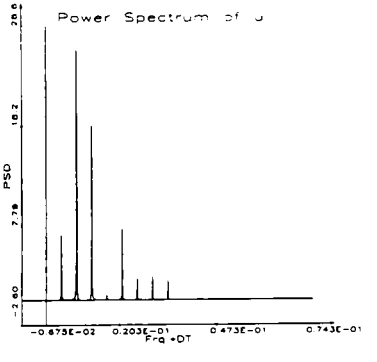

(o) Load factor $n = 2.54$

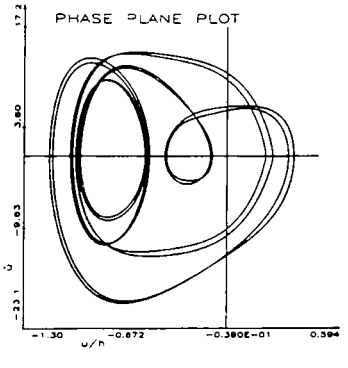

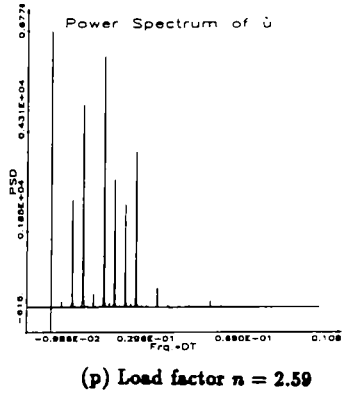

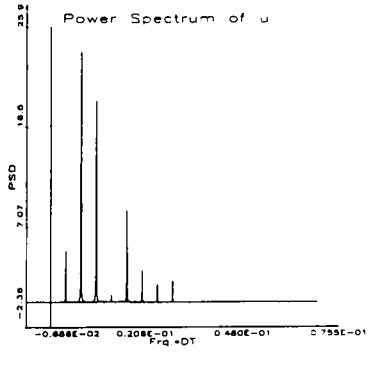

(p) Load factor $n = 2.59$

Figure 4. (continued).

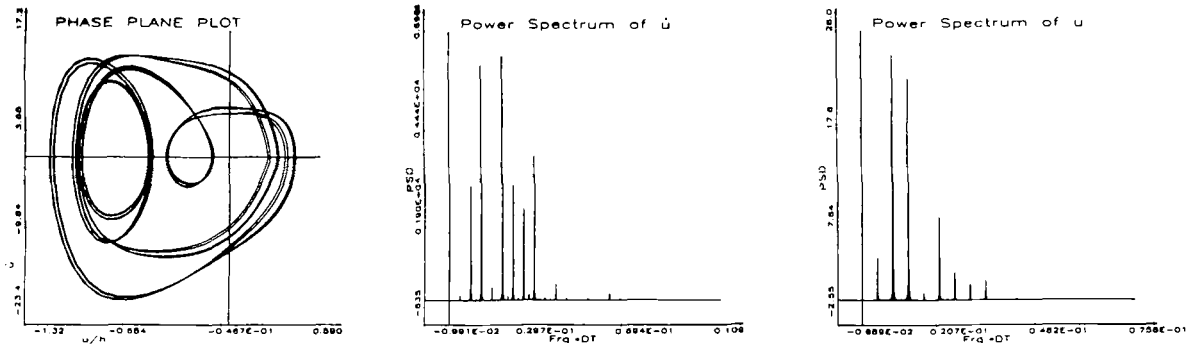

(q) Load factor $n = 2.60$

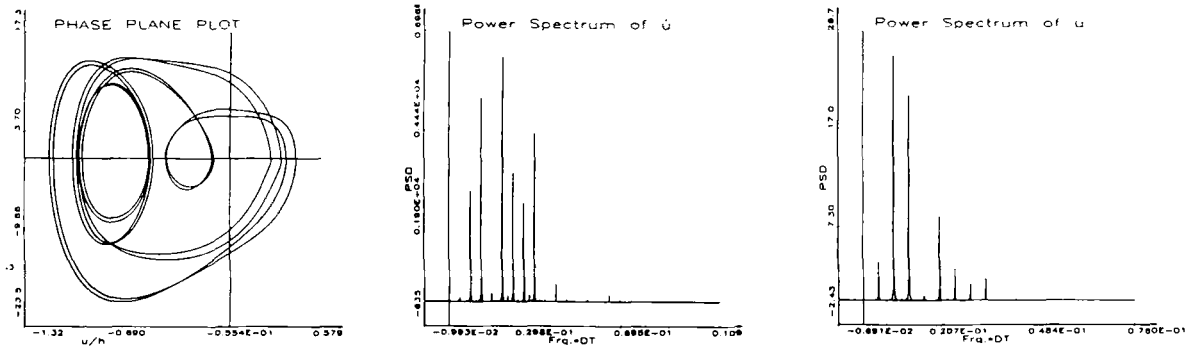

(r) Load factor $n = 2.61$

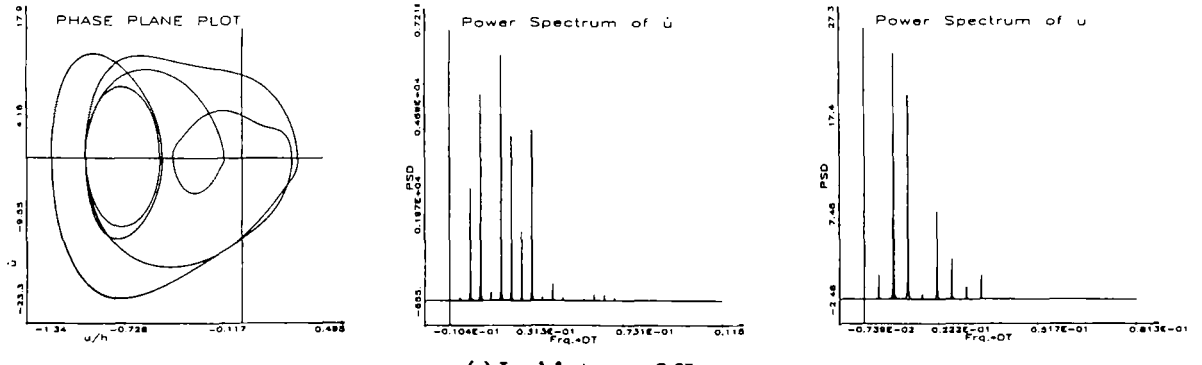

(s) Load factor $n = 2.65$

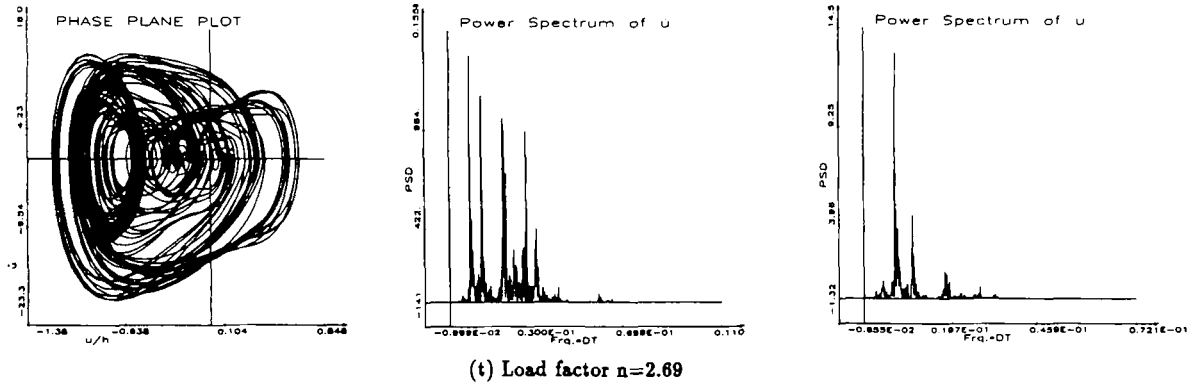

(t) Load factor n=2.69

Figure 4. (continued).

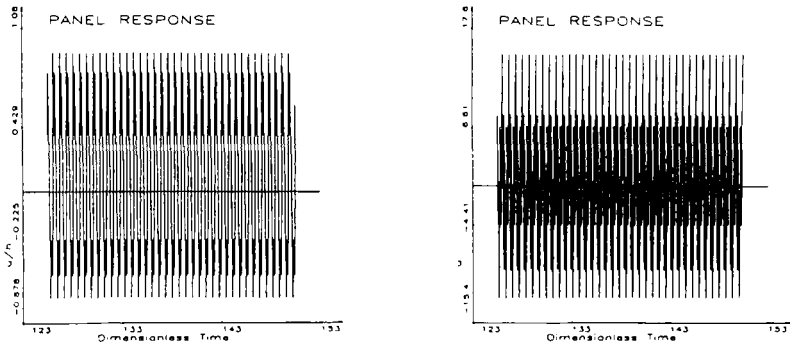

(a) Load factor $n = 1.00$

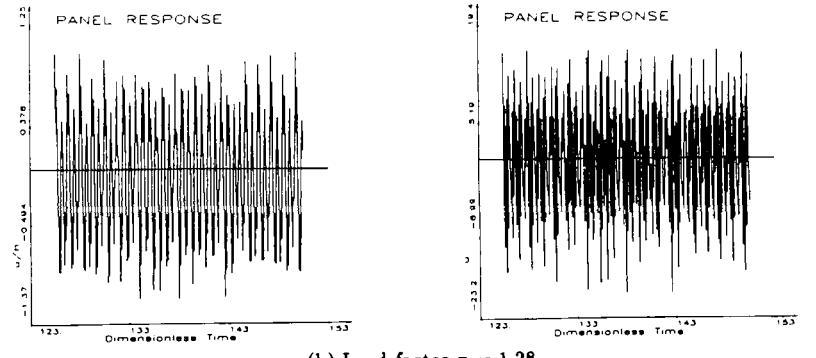

(b) Load factor $n = 1.28$

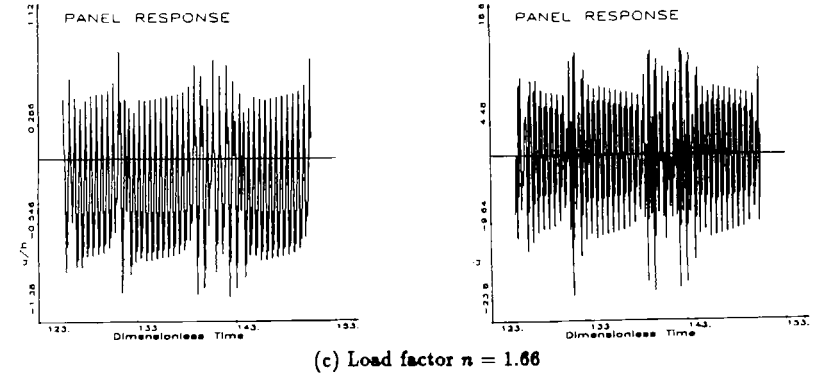

(c) Load factor $n = 1.66$

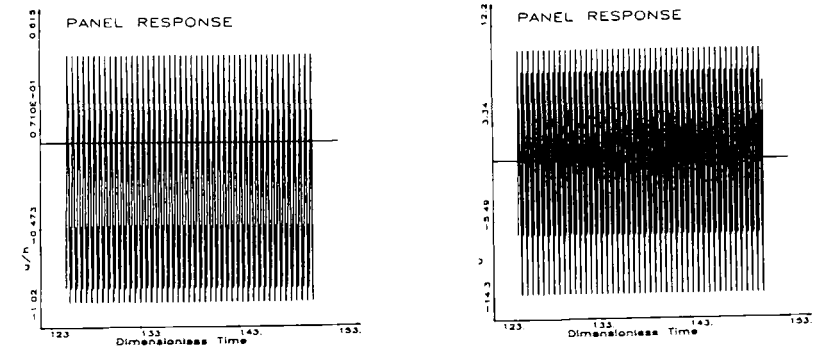

(d) Load factor $n = 1.67$

Fig. 5. Long-time history for selected cases shown in Figure 4.

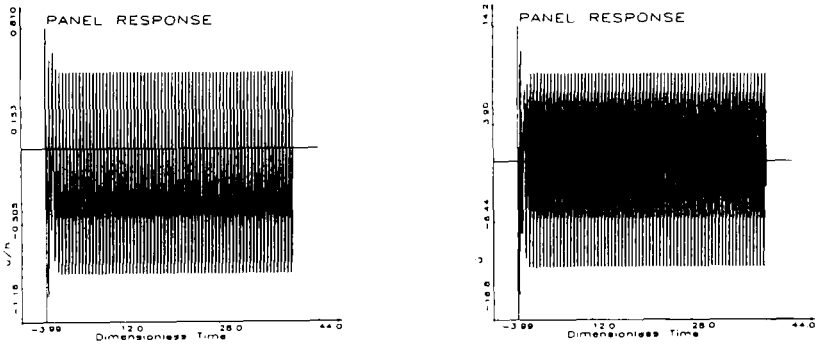

(d) Load factor $n = 1.67$

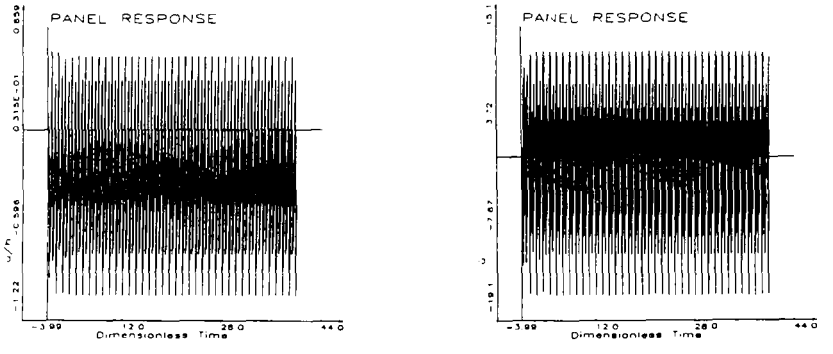

(f) Load factor $n = 1.90$

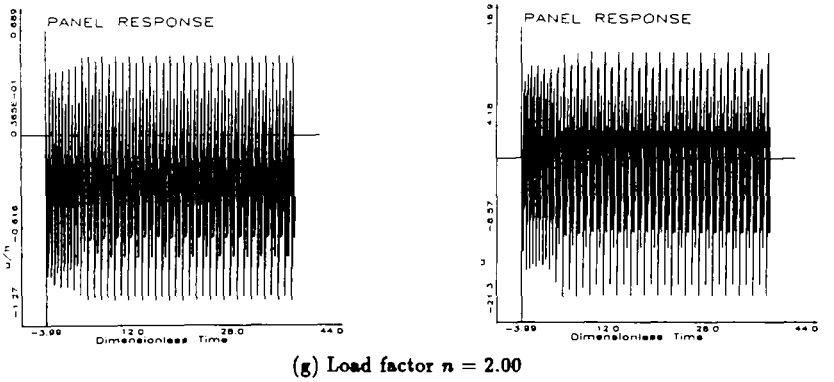

(g) Load factor $n = 2.00$

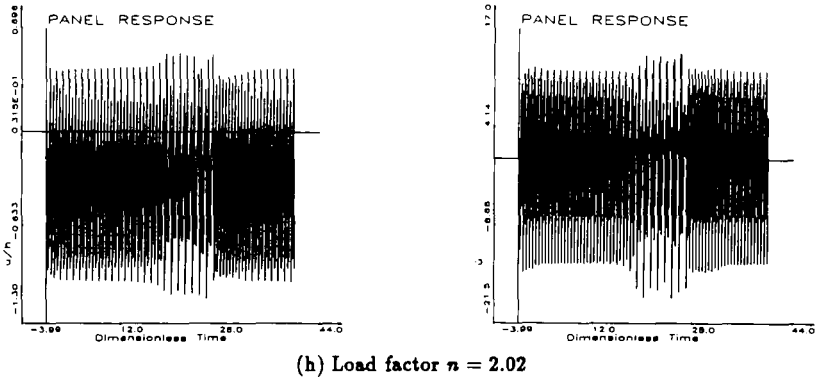

(h) Load factor $n = 2.02$

Figure 5. (continued).

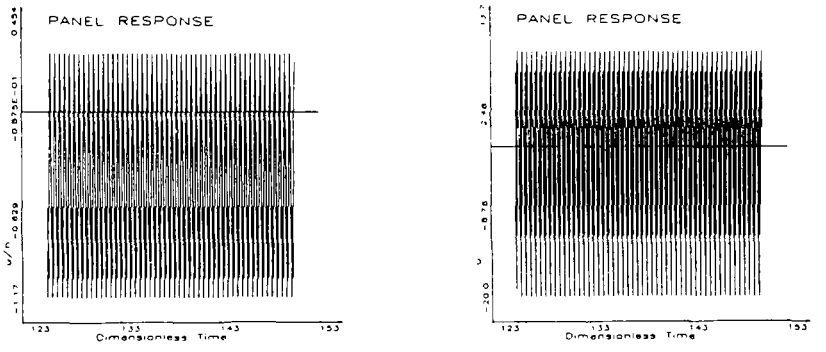

(k) Load factor $n = 2.38$

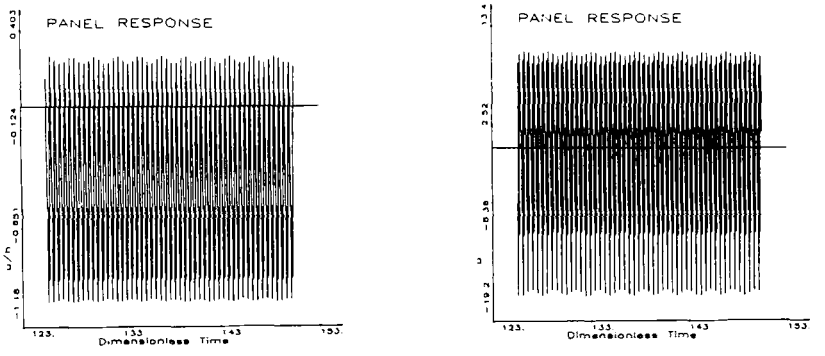

(l) Load factor $n = 2.42$

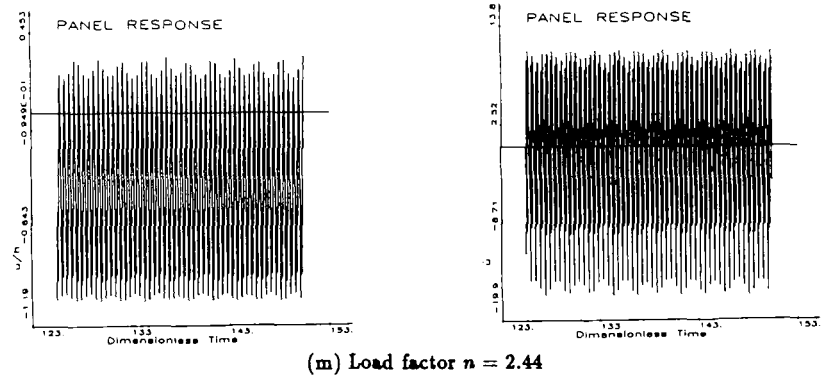

(m) Load factor $n = 2.44$

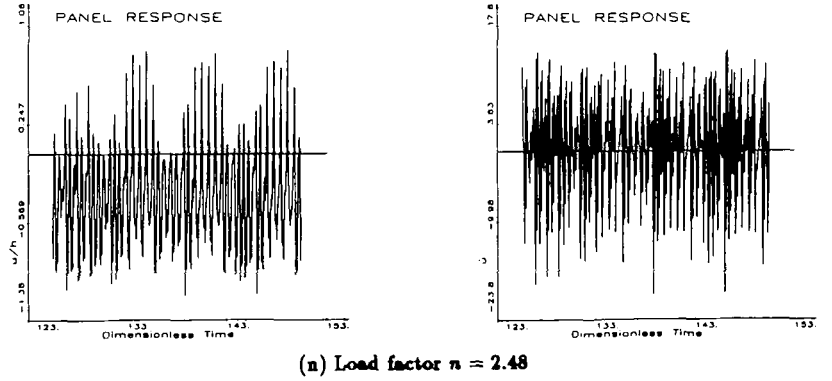

(n) Load factor $n = 2.48$

Figure 5. (continued).

period-doubling bifurcations culminating in chaos. This process is discussed in following subsection.

3.2.2. Period-Doubling Bifurcation

A cascade of period-doubling bifurcation is presented in the sequence of Figures 4(d)–4(h). The corresponding sequence of time traces is shown in the Figures 5(d)–5(h). The first bifurcation may be seen for $n = 1.83$ (see Figure 4(e)) and is well established for $n = 1.90$ (see Figure 4(f)). The usual splitting of the trajectories can be seen in the phase portrait, and time traces, see Figures 4(f), and 5(f) respectively. The spectrum also shows the bifurcation with the presence of new spectral lines. The new spectral lines show that the period has now doubled. Increasing n further causes the previous pattern to repeat; a splitting of each of the previous harmonic bands into two bands as shown in Figures 4(g) and 5(g). One anticipates that by continuing to increase n, the same phenomenon will be repeated. We expect to see a cascade of bifurcations, each accompanied by the period doubling associated with a subharmonic instability, leading to chaos. The numerical calculations support this anticipation, showing the chaotic response for $n = 2.02$.

3.2.3. The Inverse Cascade and More Chaos

We have seen that the approach to chaos via period doubling is a highly structured process. Increasing the load factor still further we have observed another element of order in the dynamic behavior of a fluttering plate, namely the inverse cascade of subharmonic bifurcations. Starting from the chaotic response for $n = 2.02$, changing of the load factor has resulted in the sequence of period-demultiplying bifurcations, see Figures 4(h)–(k), culminating in the new limit cycle, see Figure 4(k). Comparing this limit cycle with the plate response for $n = 1.00$, Figure 4(a), one can see that inertial forces due to maneuvering have suppressed the plate vibration around the up buckled position.

In the load factor range $n = 2.38$–2.48, see Figures 4(k)–(n), the above limit cycle experiences a cascade of transitions culminating in chaos. The power spectrums show large fundamental frequency components with new frequencies added to a narrow band around them, see Figure 4(m). Note that this is characteristic for the process of amplitude modulation of a periodic response. Furthermore, the time traces show the amplitude modulated periodic motion, see Figures 5(k)–(n). All this suggests the amplitude modulation as a possible route of transition from a periodic state to chaos. By the value of the load factor $n = 2.48$ the chaotic stage is well established.

For the value of the load factor in the range of $n = 2.84$–2.53, chaotic responses were observed. An unexpected limit cycle (at $n = 2.54$, Figure 4(o)) appears through a jump phenomenon; we did not observe the gradual transition through the inverse cascade of bifurcations. Upon further examinations one may conclude that this is the limit cycle that exists in the non-maneuvering case (see Figure 2), after the maneuver has suppressed one of the orbits. This limit cycle experiences a direct and inverse cascade of subharmonic bifurcations, see Figures 4(o)–(s); we did not observe chaos as a culmination of the period-doubling sequence. Further increase of the load to $n = 2.69$ transforms the plate response to chaotic through a jump phenomenon, see Figure 4(t). For the load factor in the range $n = 2.69$–2.98 the plate response is chaotic. When the load factor reaches $n = 3.00$ the inertial forces suppress the chaotic character of the motion, the response is a fixed point, and all motion ceases. As n continues to increase, the deflection of the plate increases.

3.3. *Nonautonomous Equations*

In the case when the angular velocity of maneuvering is a given function of time, the differential equations, Equation 20, are nonautonomous and they will be briefly considered in this subsection. Consider an airplane in a pull-up maneuver during the time interval (t_1, t_2). The angular velocity is given by $\omega = \omega_0 \sin[\alpha(t - t_1)]$, with $\alpha = \pi/(t_2 - t_1)$. Under these assumptions, the angular velocity at the beginning and at the end of the maneuver equals zero. For the case of $\lambda = 150$, and $R_x = -3.0\pi^2$, the non-maneuvering, $n = 1.00$, response of the plate is simple harmonic, see Figure 6(a). Constant velocity pull-up maneuver, $n = 2.00$ transforms this response into a more complicated limit cycle with two orbits, see Figure 6(b). Now consider a sinusoidal maneuver with the

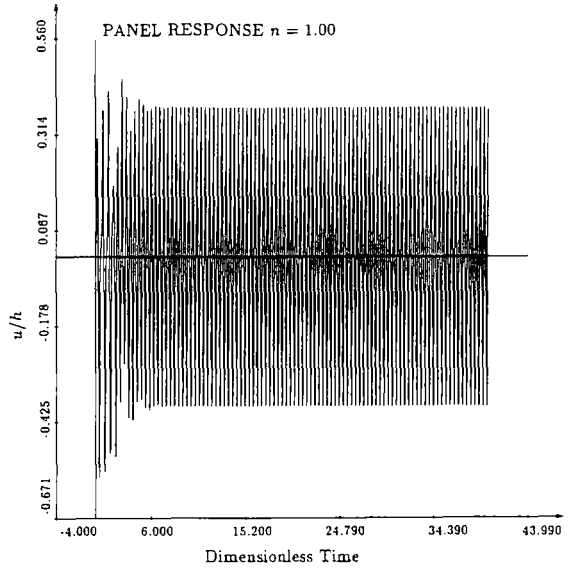

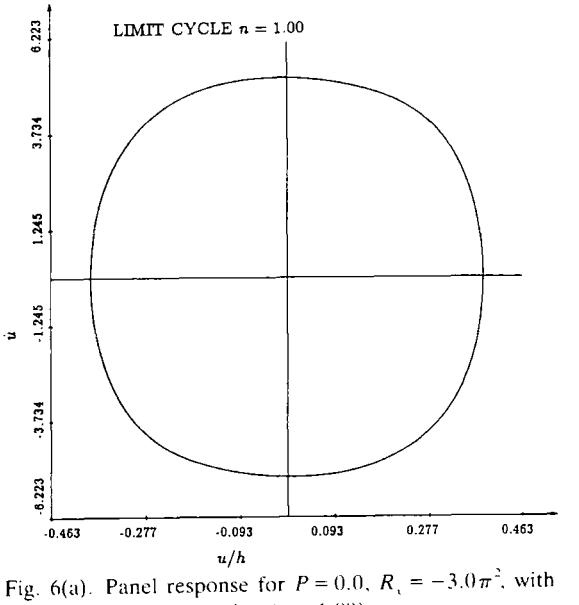

Fig. 6(a). Panel response for $P = 0.0$, $R_x = -3.0\pi^2$, without maneuvering ($n = 1.00$).

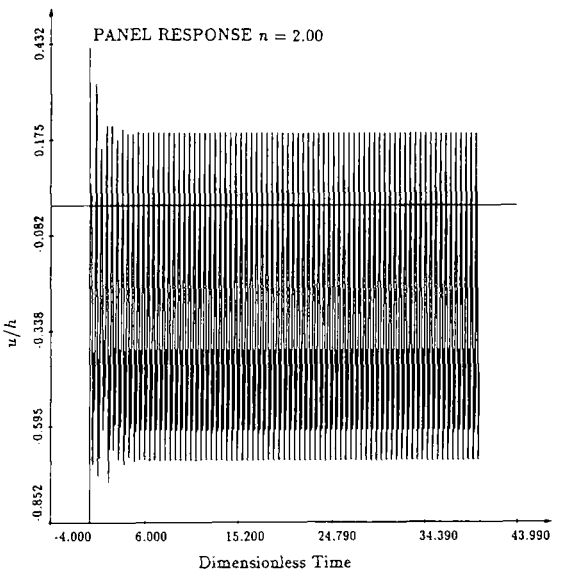

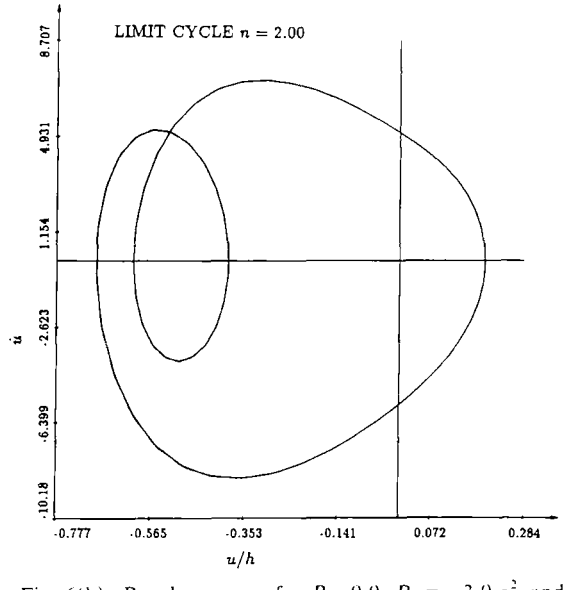

Fig. 6(b). Panel response for $P = 0.0$, $R_x = -3.0\pi^2$, and constant velocity pull-up maneuver ($n = 2.00$).

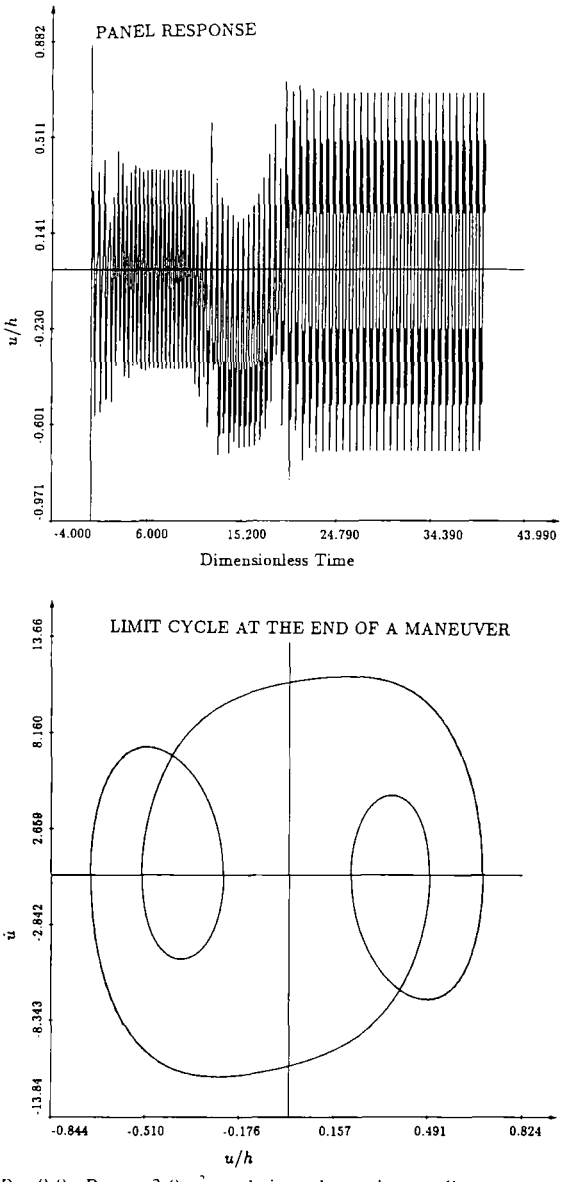

Fig. 6(c). Panel response for $P = 0.0$, $R_v = -3.0\pi^2$, and time dependent pull-up maneuver (amplitude $n = 2.00$).

amplitude $n = 2.00$. As might be expected on physical grounds, our calculations show a disturbance of the simple harmonic limit cycle by the inertial forces due to the maneuver. The remarkable results appear after the completion of the maneuver, when the panel motion is a more complicated limit cycle with three closed orbits in evidence, see Figure 6(c). In order to understand this result, note that the conditions at the end of the maneuver correspond to the initial conditions for the non-maneuvering continuation of the flight. It is then apparent that the presence of maneuvering has moved the initial conditions into a basin of the attraction of the new attractor. In some regions of the initial condition space one may expect even more dramatic changes of the dynamical behavior due to time dependent maneuver, especially close to the boundaries of the basin of attraction. It is clear that this study has to be related to the analysis of the influence of initial conditions. This may be a subject of future research.

4. Concluding Remarks

A Lagrangian mechanics formulation in the rotating frame of reference for the aeroelastic analysis of a fluttering plate of a maneuvering aircraft has been derived. The formulation includes geometric non-linearities associated with the occurrence of tensile stresses in the middle surface, as well as the effect of the rigid-body rotation on the other degrees of freedom. The general response of the system were simulated on the digital computer by using a fourth-order Runge–Kutta algorithm. Long-time histories, phase plane plots, and power spectra have been used to characterize the responses.

We have chosen system parameters such that there are two equilibrium positions for the non-maneuvering case. The numerical simulations for periodic and chaotic responses are conducted in order to analyze the influence of maneuvering on the dynamic behavior of the panel. It was shown that chaos could occur in a maneuvering case for system parameters in the actual flight range. The presence of a load factor n can transform the response from the fixed point into a simple periodic or even chaotic state. It can also suppress the periodic character of the motion, transforming the response into a fixed point, so that all motion ceases.

For the base case of $\lambda = 150$, and $R_x = -3.5\pi^2$, the load factor was varied from the non-maneuvering response to a value for which the inertial forces due to the maneuver suppress the plate motion, in order to study the mechanisms through which the transition between periodic and strange attractors occurs. As the maneuver (load factor) increases, the system exhibits complicated dynamic behavior including a direct and inverse cascade of subharmonic bifurcations, intermittency, and chaos. Beside these classical routes of transition from a periodic state to chaos, our calculations suggest amplitude modulation as a possible new mode of transition to chaos. In the case of a prescribed time dependent maneuver, a remarkable transition between the different types of limit cycles is presented. The results indicate that the study of this deterministic system is important from the practical, and theoretical viewpoint. First, the fact that maneuvering can change the character of the panel response is of practical interest to aeroelasticians as it affects, for instance, fatigue analysis. Secondly, the techniques employed in this study can be extended to the problem of aeroelasticity of aircraft (with all non-linearities geometric, dynamic, and aerodynamic included). From the theoretical point of view, this physical system is a rich source of static and dynamic instabilities and of associated limit-cycle motions and it could be used for instance as a test case for assessing techniques for the study of nonlinear dynamics and chaos.

Subjects for consideration in future research include the use of other stability concepts such as Liapunov exponents, and Poincaré maps. Application of complementary methods of differentiable dynamics, in particular, of center manifold and bifurcation theory, to analyze the problem from a qualitative viewpoint would be helpful. Knowledge of generic structures of attracting sets in N-space, might make the interpretation of numerical solutions of evolution equations considerably clearer.

Acknowledgements

Research sponsored by the Air Force Office of Scientific Research (AFSC), under Contract No. F49620-86-C-0040. The United States Government is authorized to reproduce and distribute reprints for governmental purposes notwithstanding any copyright notation herein. The author wishes to thank Dr. Anthony K. Amos of the Air Force Office of Scientific Research, Mr. Carey

S. Buttrill of NASA Langley Research Center, Professor Luigi Morino of the University of Rome, and Professors Guido Sandri and Marvin Freedman of Boston University for valuable discussions on this work.

References

1. Bisplinghoff, R. L. and Ashley, H., *Principles of Aeroelasticity*, Dover, 1962.
2. Bolotin, V. V., *Nonconservative Problems of the Theory of Elastic Stability*, Pergamon Press, 1963.
3. Dowell, E. H., 'Nonlinear oscillations of a fluttering plate', *AIAA Journal* **4** (7), 1966, 1267–1276.
4. Dowell, E. H. and Ilgamov, M., *Studies in Nonlinear Aeroelasticity*, Springer-Verlag, 1988.
5. Dowell, E. H. and Pezeshki, C., 'On the understanding of chaos in the Duffing's equation including a comparison with experiment', *Journal of Applied Mechanics* **52**, 1986, 949–957.
6. Holmes, P. J. and Marsden, J., 'A partial differential equation with infinitely many periodic orbits: Chaotic oscillations of a forced beam', *Archives for Rational Mechanics and Analysis* **76**, 1981, 135–166.
7. Paolozzi, A., Peroni, I., and Sipcic, R. S., 'Analisi della stabilità e comportamento chaotico di sistemi aeroelastici', in *Proceedings of the X Congresso Nazionale AIDAA*, Pisa, Italy, Oct. 16–20, 1989.
8. Pezeshki, C. and Dowell, E. H., 'An examination of initial condition maps for the sinusoidally excited buckled beam modeled by the Duffing's equation', *Journal of Sound and Vibration* **117** (2), 1987, 219–232.
9. Pezeshki, C. and Dowell, E. H., 'On chaos and fractal behavior in a generalized Duffing's system', *Physica D* **32**, 1988, 194–209.
10. Zavodney, L. D. and Nayfeh, A. H., 'The response of a single-degree-of-freedom system with quadratic and cubic non-linearities to a fundamental parametric resonance', *Journal of Sound and Vibration* **120** (1), 1988, 63–93.
11. Zavodney, L. D., Nayfeh, A. H., and Sanchez, N. E., 'The response of a single-degree-of-freedom system with quadratic and cubic non-linearities to a principal parametric resonance', *Journal of Sound and Vibration* **129** (3), 1989, 417–442.
12. Sipcic, R. S. and Morino, L., 'Chaotic response of fluttering panel, the influence of maneuvering', Technical Report 89-1, Boston University, Boston, 1989.
13. Sipcic, R. S. and Morino, L., 'Dynamical behavior of the fluttering panel on a maneuvering airplane', to appear in *AIAA Journal*, 1990.
14. Yano, S., 'Parametric excitation in a self-exciting system (1st report)', *Bulletin of the Japan Society of Mechanical Engineers* **27**, 1984, 2483–2491.
15. Yano, S., 'Parametric excitation in a self-exciting system (2nd report)', *Bulletin of the Japan Society of Mechanical Engineers* **28**, 1985, 483–491.